Highly Localized C-N2 Sites for Efficient Oxygen Reduction

Qiangjian Ju,[1,6] Ruguang Ma,[1,] Yifan Hu,[1,6] Beibei Guo,[1] Qian Liu,[1,2] Tiju Thomas,[4] Tao Zhang,[1] Minghui Yang,[2,3] Wei Chen,[5] and Jiacheng Wang[1,2,]**

[1]The State Key Laboratory of High Performance Ceramics and Superfine Microstructure, Shanghai Institute of Ceramics, Chinese Academy of Sciences, 1295 Dingxi Road, Shanghai 200050, China

[2]Center of Materials Science and Optoelectronics Engineering, University of Chinese Academy of Sciences, Beijing 100049, China

[3]Ningbo Institute of Materials Technology and Engineering, Chinese Academy of Sciences, 1219 Zhongguan West Road, Ningbo 315201, China

[4]Department of Metallurgical and Materials Engineering, Indian Institute of Technology Madras, Adyar, Chennai 600036, Tamil Nadu, India

[5]Department of Mechanical, Materials and Aerospace Engineering, Illinois Institute of Technology, Chicago, IL 60616, USA

[6]University of Chinese Academy of Sciences, 19A Yuquan Road, Shijingshan District, Beijing 100049, China

KEYWORDS: electrocatalysis, oxygen reduction reaction, triazine ring, electronic structure, metal-air battery

ABSTRACT: Searching for oxygen reduction reaction (ORR) catalysts outperforming Pt, the state of the art material, continues. Doped carbon-based materials offer a viable means for replacing Pt, but their activity improvement still remains great challenge. Here configurations of N-doped carbons are firstly analyzed using *ab* initio simulations towards ORR. The results show that a certain short-range ordered structure labeled as C-N2, which comprises of two nitrogen atoms flanking carbon, is the optimal choice. The predicted configuration of C-N2 is experimentally realized by triazine-doped carbon (triNC). The triNC with C-N2 sites demonstrates high ORR activity (onset potential 0.98 V, halfwave potential 0.89 V) comparable to commercial 20% Pt/C. The highly localized and positive charged carbon atom in C-N2 structure facilitates the dissociation of O_2 to increase the ORR kinetics, proved by theoretical calculation. A Zn-air cathode is fabricated using the triNC ORR electrocatalyst and outperforms the cathode using Pt/C in terms of specific capacity, energy density, and long-term durability. The atomic scale approach reported here provides a good strategy to achieve active carbon-based electrocatalysts for potential and scalable use in energy conversion and storage.

1. Introduction

Oxygen reduction reaction (ORR) is one of the most important electrochemical reactions in advanced energy storage and conversion devices (e.g. metal-air batteries and fuel cells). In fact, the ORR reaction is a crucial determinant of energy efficiencies of these devices.[1-2] Furthermore the ORR rates determine the power densities of the corresponding devices. The state-of-art ORR electrocatalysts are Pt-based materials. However, the high cost and poor availability of Pt-group elements limit their applications in industry.[3] Hence extensive efforts are being devoted to develop noble metal free electrocatalysts.[4-7] In this context, carbon-based materials are regarded as potential metal-free electrocatalysts for ORR due to their low cost, high conductivity and rather facile tunability of their electronic structure.[8-9]

Heteroatom doping (e.g. N, P, S and so on) has been shown to be one of the most effective methods to activate the carbon scaffold towards improved ORR activity.[8-11] In particular, N-doping has been widely studied.[12-29] Using model catalysts and first principles calculations, it has been shown thus far that enhanced ORR performance correlates with carbon sites that have a significant positive charge, high spin density, unsaturated coordination and so on.[16, 30-36] This recent insight offer fresh directions for atomic scale design of new carbon materials with improved catalytic activities.

Very few different active, N-containing species have been proposed during the past decade.[5] This remains true even since an N-doped carbon material was firstly reported as an ORR catalyst.[12] Of note are reports on pyridine N (pyri-N), graphitic N (grap-N), pyrrolic N (pyrr-N) and oxide-N.[15] In most cases, the ORR activity of N-doped carbon materials is simply attributed to high amounts of pyri-N and N doping is usually considered as an isolated single N atom doping. [13, 37] However, it is found that different carbon materials with similar nitrogen amounts show great discrepancy in ORR performance. Importantly the influence of chemical environment of carbon site for ORR has not been sufficiently explored. In particular, short-range ordered structures could offer means to modify the character of carbon more efficiently than randomly introduced N-doping does.

Herein, density functional theory (DFT) based calculation is carried out to explore the ORR performance at a carbon site. Different coordination environments for the carbon are explored. We find that the coordination environment significantly impacts the character of the carbon site. In particular, the positive charge associated with the carbon site and the corresponding oxygen binding energy is found to be optimum for a configuration labeled as C-N2 (carbon site with two adjacent N atoms). Thereafter, for the experimental realization, a covalent triazine framework (CTF) material is chosen as a precursor to synthesize the target material. The materials obtained thus have the unique triazine ring structure (C3N3), which can be seen as a superstructure of three pyri-N doping, consisting of three C-N2 sites. As-synthesized triazine ring doped carbon (triNC) outperforms traditional N-doped graphene (N-G) and commercial Pt/C toward ORR, proving that it is a powerful candidate for metal free ORR electrocatalyst. As a demonstration of its performance, an air cathode is fabricated using the triNC electrocatalyst and used in the assembly of a Zn-air battery. The device shows superior specific capacity, energy density, and durability when compared to the system that uses commercial Pt/C. Our work shows good combination of theoretical prediction and experimental performances, leading to an in-depth method for studying carbon material toward ORR and other electrocatalytic reactions.

2. Result and Discussion

DFT calculations are performed to predict the atomic configurations in N-doped carbon scaffolds that can offer optimum ORR activity. As shown in Figure 1a-b and Figure S1a-b, two different nitrogen coordination conditions are studied. The carbon sites which are adjacent to one and two nitrogen atoms are named as C-N and C-N2 sites, respectively. The calculated C-N site and C-N2 site are located at pyri-N doped carbon and the triazine structure (C3N3), respectively.[38-39] Doping with N atoms could increase the electron transfer from C to N, resulting in the creation of positive C sites. The valence state of each atom is measured by the Bader charge analysis. It is clearly seen that the C site next to an N atom has a positive charge (Figure 1a-b). Furthermore, the C-N2 site (i.e. the C site flanked by two N atoms) has a much more positive charge than the C-N site (1.06~1.07$|e^-|$for C-N2 and 0.53$|e^-|$ for C-N). Based on reports thus far, it is reasonable to say that the ORR activity originates from carbon sites that have positive charges.[15] Positive charged C site would influence the chemical adsorption mode of O_2 molecule, as well as other intermediate of ORR and leads to better ORR performances.[12, 34, 40-42] This implies the possibility of superior ORR activity with C-N2 when compared to C-N sites.

Furthermore, the electronic structures of C-N and C-N2 sites and corresponding oxygen binding characteristics are analyzed. Figure 1c-d and S2a-b are the density of states (DOS) plots of the C-N and C-N2 sites. Both C-N and C-N2 sites present typical sp^2 hybridization with three orbitals contributing to lower energy levels (s, p_x and p_y) and one orbital yielding the higher energy levels (p_z). Compared with the p_z orbital of C-N, the one in C-N2 presents a much higher degree of localization. The DOS of the p_z orbital results in splitting atomic energy state (splitting peaks) instead of continuous crystal bands. This indicates that the N atoms that surround the C site result in a reduction of C-C interaction and C-C bonds in graphite. In case of the C atom in the C-N2 site, it is almost becomes like a "stand-alone single atom" instead of one that is strongly embedded in graphitic carbon. This localization makes C in C-N2 more like a "single atom catalyst" (SAC, such as Fe-N_4),[43] even though it is not a metal atom. This is relevant since a former report has also pointed to the fact that the localization of carbon affects the oxygen binding energy and further influences the ORR performance.[22] The increased localized DOS could lead to the better field-emission property. The electron of highly localized C can be excited in sufficient voltage, which benefits the electron transfer between electrode and O_2, as well as oxygen reduction reaction. [34, 44-45]

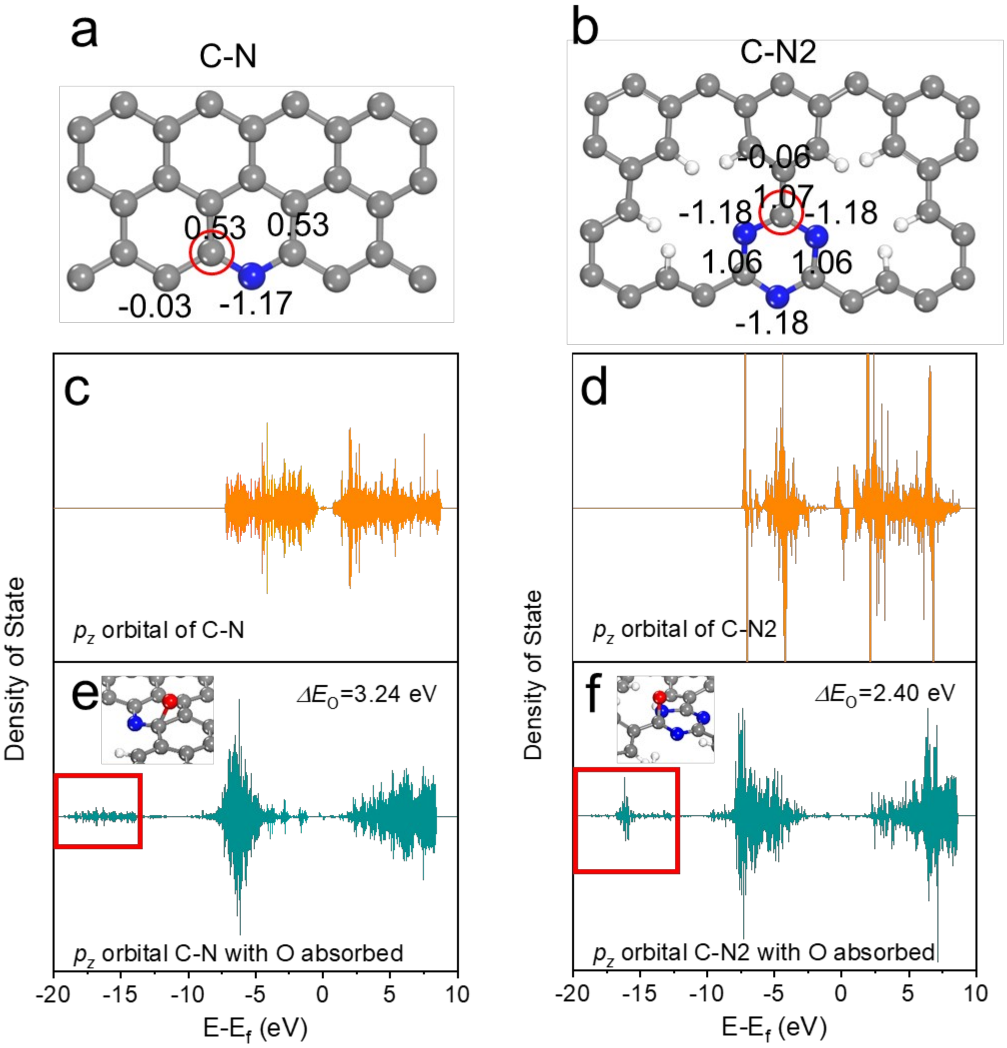

Figure 1. DFT calculation on carbon materials with different kinds of active carbon sites. Structure of carbon materials with: (a) pyri-N doping (C-N) and (b) triazine ring doping (C-N2). Red circles are used to point to the atoms forming the active sites. The data given refers to the valence state of the corresponding atoms analyzed using the Bader charge analysis. pDOS of p_z orbitals of C-N site and C-N2 site: (c-d) without O adsorption and (e-f) with O absorption. Inserts of (e) and (f) refer to the enlarged part of C-N and C-N2 structures with O absorption. Grey, blue, red and white spheres represent C, N, O and H atoms, respectively.

To analyze the difference of oxygen binding property between localized C-N2 site and C-N site, the DOS of the C-N and C-N2 sites after oxygen adsorption and the corresponding oxygen binding energy (ΔE_O) are further calculated (Figure 1e-f and Figure S1e-f). For the C-N2 site, it is clearly seen that a section of DOS shifts to the lower energy states (pointed by red box). This indicates an increase in the oxygen binding strength (Figure 1d). Meanwhile, for the C-N site, the intensity of the binding state is much weaker than that of C-N2.[46] This difference is also reflected in ΔE_O. C-N2 has a much higher oxygen binding strength (ΔE_O= 2.40 eV) compared to C-N (ΔE_O = 3.24 eV). Based on the Sabatier principle, the adsorption of intermediate on the catalytic surface should neither be too strong nor too weak.[47] The optimal value of ΔE_O for ORR is about 1.81 – 2.88eV;[15, 48] this is very consistent with that observed for the C-N2 site. The result hence clearly indicates that the C-N2 site offers higher ORR activity, when compared to the C-N site in pyri-N group. Above all, the unique two nitrogen coordination leads to an isolated and positive charged carbon site, and further influences the oxygen binding property. Compared with C-N, C-N2 exhibits stronger oxygen bonding strength which could facilitate the dissociation of oxygen molecule during the ORR process. This offers a means for atomic scale engineering that can yield enhanced performance from doped carbon.

Motivated by DFT calculations, triazine-ring doped carbons with C-N2 sites are synthesized as ORR electrocatalysts (Figure 2a and supporting information).[38-39, 49-50] A covalent triazine framework material is synthesis through ionothermal method. Further carbonization of CTF results in the formation of triazine-ring-doped carbon material (triNC) with C-N2 sites. The samples are named as triNCX (X refers to the carbonization temperature, 700-1200°C). ‘triNC’ mentioned here on stands for triNC1100 (except in figures and captions). For comparison, N-doped graphene (N-G) is synthesized using mechanical exfoliation and subsequent thermal treatment in ammonia (to introduce N doping and C-N sites; see details in SI).

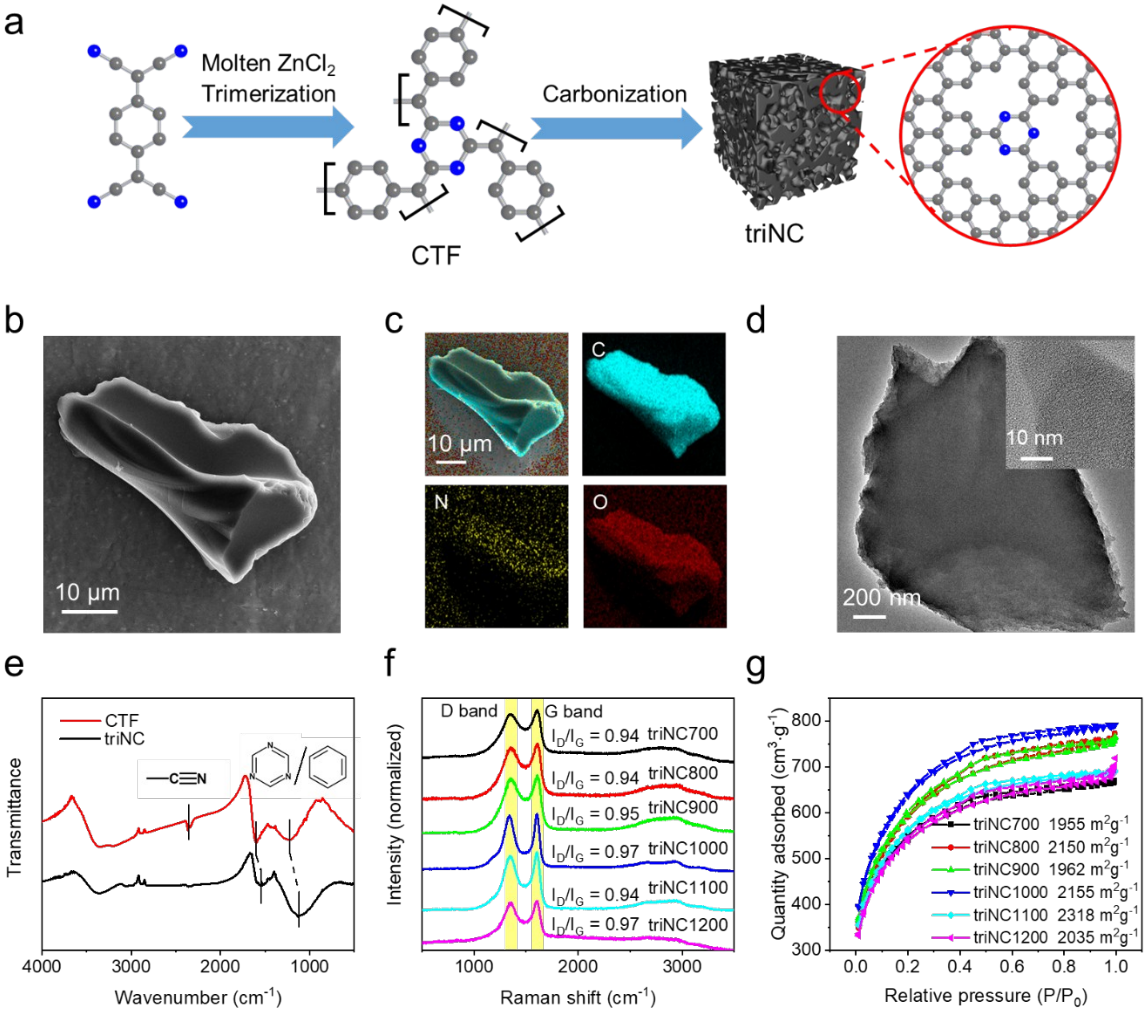

Figure 2. Synthesis and characterization of triNC. (a) Illustration of synthesis of triNC with C-N2 sites. (b) SEM image of triNC and (c) corresponding EDS mapping. (d) TEM images of triNC. Insert shows the corresponding HRTEM image of triNC. (e) FTIR spectra of CTF and triNC, and (f-g) Raman spectroscopy and nitrogen adsorption/desorption isotherms of all triNCs.

The as-synthesized triNC is studied using scanning electron microscope (SEM) and transmission electron microscope (TEM). As shown in Figure 2b and 2d, triNC particles have smooth surfaces and are several micrometers in size. N is found to be uniformly distributed in the bulk, confirmed by energy dispersive spectrometer (EDS) mapping (Figure 2c). The O element is also observed, indicating the presence of the adsorbed O species. In the high-resolution TEM (HRTEM) image (insert of Figure 2d), no clear lattice fringes could be seen, demonstrating its amorphous structure. The existence of triazine ring is confirmed using Fourier Transform Infrared Spectroscopy (FTIR). In Figure 2e, the adsorption peak at ~2200 cm^{-1} corresponds to the -C≡N stretching vibration in CTF.[51] This peak disappears after pyrolysis, indicating the successful thermal decomposition of the cyan group. The adsorption peaks at ~1560 cm^{-1} and ~1180 cm^{-1} are ascribed to the vibrations in triazine and benzene. This proves that triazine ring has indeed been doped into the carbon matrix.[38, 52]

The Raman spectra of triNCs (Figure 2e) reveal patterns typical of disordered carbon materials.[53-54] The intensity ratio associated with D and G bands (I_D/I_G) for triNC samples remains stable (about 0.94-0.97). This indicates that the degree of carbonization does not change with annealing temperature. This is typical for organics-derived carbon materials (so called hard carbon materials).[55] The specific surface area (SSA) of triNC is evaluated using nitrogen isothermal adsorption/desorption measurement. As shown in Figure 2g, all triNC samples reveal reversible type I loops, indicating the existence of both micropores and mesopores. The pore size distribution is analyzed by nonlocal density functional theory (NLDFT, Figure S3).[56] The pores are typically beyond 10 nm, proving the existence of a hierarchically arranged micro-mesoporous structure. The microporous structure mainly originates from the amorphous triazine-ring structure and the carbon defects next to triazine ring. All triNC samples reveal a high Brunauer-Emmett-Teller (BET) SSA of ~2000 m^2 g^{-1}. Similar to triNCs, the morphology and feature of N-G are characterized, revealing the formation of N-doped few layer graphene with a similar SSA as that of triNC (see details in supporting information, Figure S4-S6).

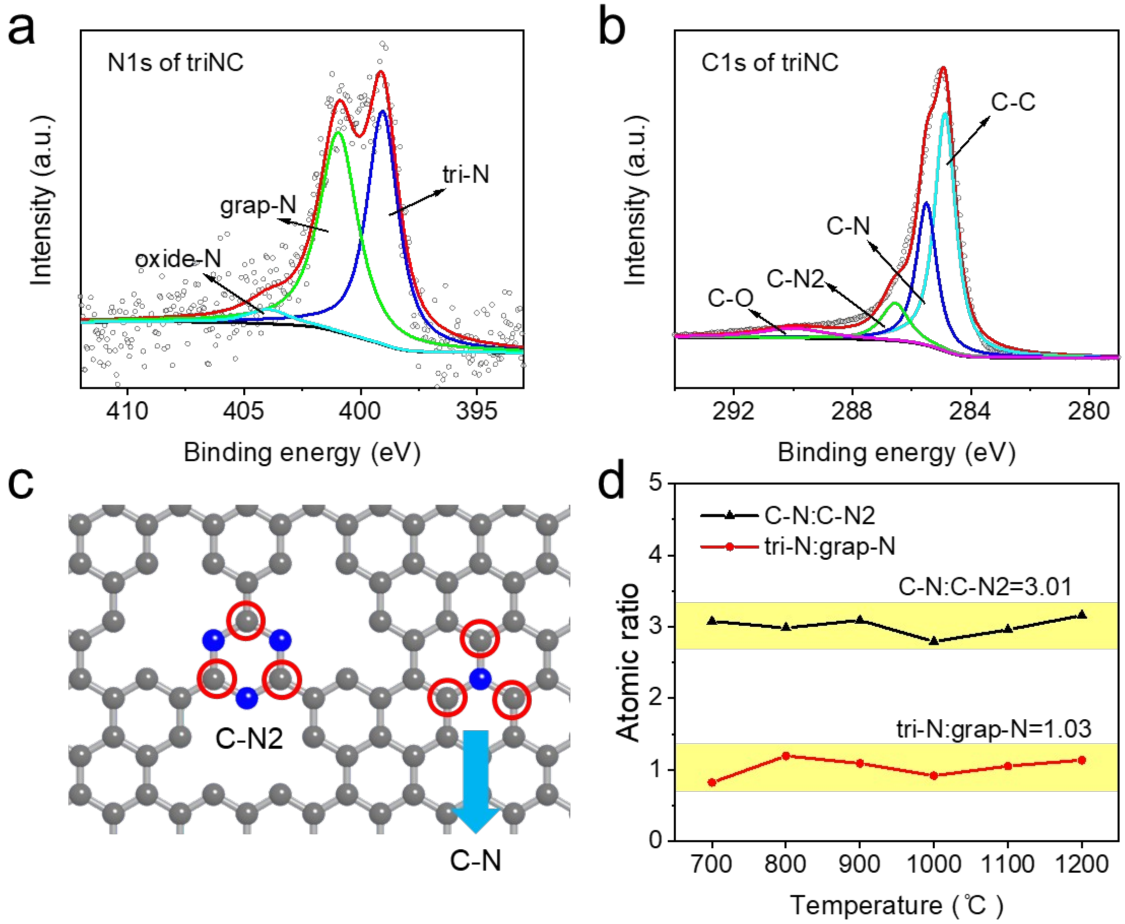

Figure 3. XPS measurement of triNC. High resolution XPS spectra of (a) N1s and (b) C1s of triNC. (c) Predicted structural model of triNC. (d) Atomic ratio of C-N : C-N2 and tri-N : grap-N.

X-ray photoelectron spectrum (XPS) is measured to detect the elemental compositions and chemical environments of all triNCs. The XPS survey spectra are shown in Figure S7. In the survey spectrum of triNC700, peaks of residual $ZnCl_2$ are clearly observed. With the increase of annealing temperature, only peaks of C, N and O are observed. The contents of Zn are less than 0.1 at% (Table S1), indicating that the residual $ZnCl_2$ is removed. As shown in Figure 3a and Figure S8, the N1s high-resolution spectra of all triNCs prepared at different carbonization temperatures can be deconvoluted into three peaks. The peak at ~398.8 eV corresponds to the triazine-N atoms (tri-N). This indicates that triazine ring is preserved even after carbonization at high temperature.[38] The peak at ~402.2 eV shows the presence of grap-N, caused by carbonization of some unstable triazine rings. Similarly, the high-resolution spectrum of C1s could be deconvoluted into four peaks, reflecting the chemical environments of the C atoms (Figure 3b and Figure S9). The main peak at ~284.8 eV represents the graphitic sp^2 C-C. Two peaks located at ~285.7 eV and ~287.0 eV are assigned to the C atom with one and two adjacent N atoms, respectively. One weak peak at ~290.2 eV reflects the presence of the C-O bond. The differences of XPS peaks of three C site (C-N2, C-N and C-C) are further confirmed by DFT calculation. The calculated core level eigenenergies of 1s electron are -270.4 eV for C-N2, -269.0 eV for C-N and -268.2 eV for C-C, respectively. It is clearly revealed that the neighboring N atoms deepen the eigenenergies of C 1s electron. This caused the increase of C 1s binding energy for C-N and C-N2 sites compared with C-C, confirming the C 1s XPS results.

Given the above, it is clear that the triNC samples contain both grap-N and triazine ring structure, schematically represented in Figure 3c. The corresponding C-N and C-N2 sites are pointed in red circles. In triazine ring structure, the ratio of C-N2 and tri-N is 1:1 (three C-N2, as well as three tri-N atoms). In grap-N, one N atom has three neighboring C-N sites and the ratio of C-N and grap-N is 3:1. Therefore, the ratio of C-N : C-N2 is supposed to be three times that of the ratio of tri-N : grap-N. The relevant contents of C-N, C-N2, tri-N and grap-N are analyzed by studying the area of corresponding peaks (Figure 3d). The average ratios of C-N : C-N2 for all triNC samples remain 3.01 (on an average). This is three times the ratio of grap-N (~1.03 on average), matches well with our assumption and confirms the existence of C3N3/C-N2 structure.

Similar to triNC, N-doped graphene (N-G) is analyzed using XPS. As shown in Figure S10 and Table S1, only C, N and O elements occur in N-G. The total N content reaches 8.5 at% in this sample. The high-resolution N1s spectrum can be deconvoluted into four peaks which are pyri-N (398.8 eV), pyro-N (400.2 eV), grap-N (401.6 eV) and oxide-N (404.0 eV). It is clearly seen that the pyri-N is dominated by N species in N-G (pyri-N: 45.1 at%, pyro-N: 25.8 at%, grap-N: 25.6 at% and oxide-N: 3.5 at%). C1s spectrum can be deconvoluted into three peaks (C-C, C-N and C-O). No C-N2 peak is observed, indicating that the short-range ordered structure is not formed through thermal treatment in NH_3 atmosphere.

To further detect the distinctions in the coordination environments of C, the C^{13} solid state nuclear magnetic resonance (SSNMR) was conducted for CTF, triNC and N-G. As shown in Figure S11. The SSNMR spectrum of CTF shows two obvious widened peaks located at around -130 ppm and -155 ppm, corresponding to the C-N/C-C coordination and C-N2 coordination, respectively.[57] The triNC exhibits the similar SSNMR spectrum as CTF, indicating the remaining of C-N2 site after carbonization. Notably, the peak of around -150 ppm does not exist in the spectrum of N-G, showing the high-temperature treatment in ammonia couldn't form the C-N2 sites.

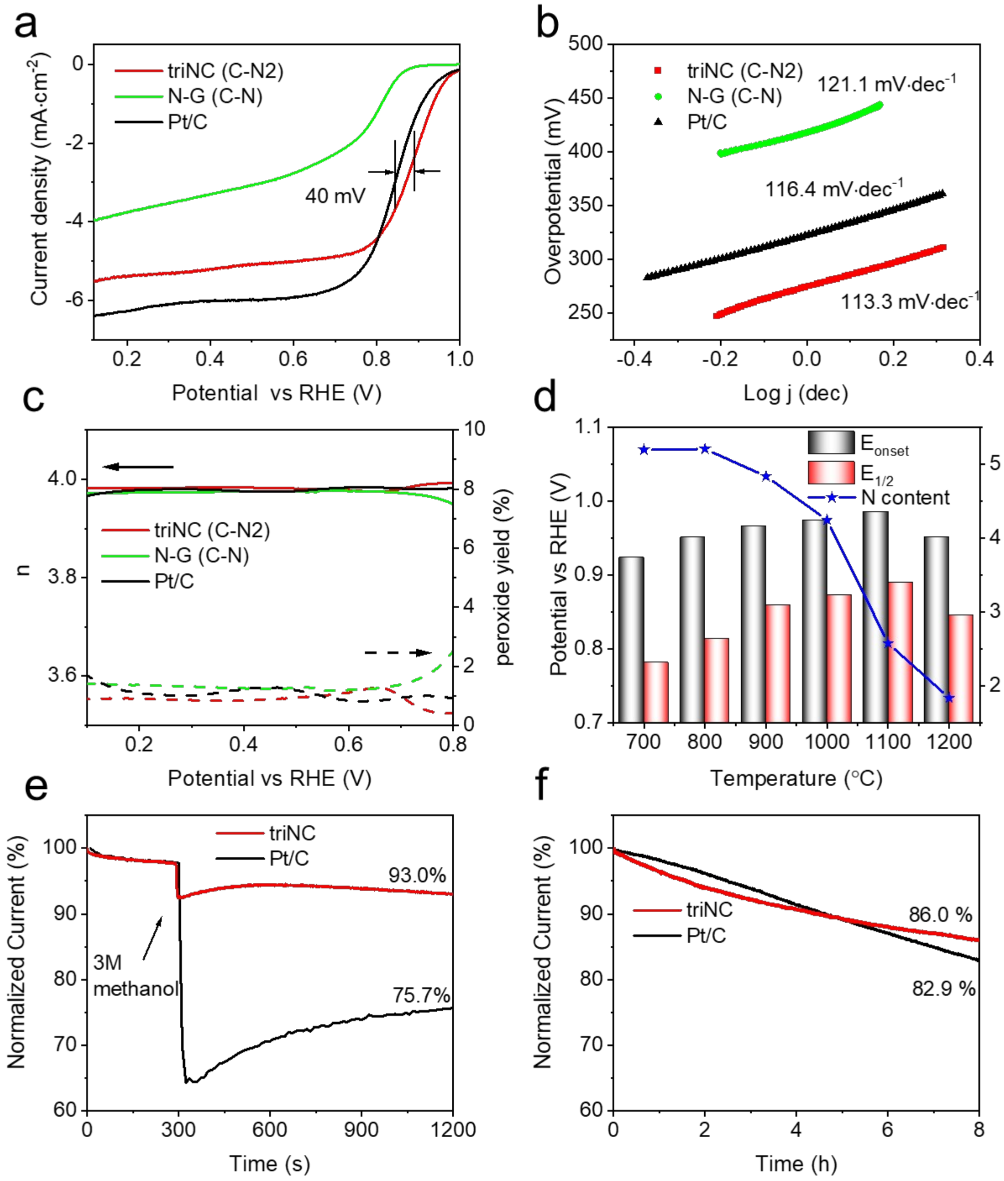

Figure 4. Comparison of ORR activities of triNC, N-G and commercial Pt/C. (a) LSV curves in O_2-saturated 0.1 M KOH solution (scan rate: 5 mV s^{-1}, rotating speed: 1600 rpm) and (b) corresponding slopes of Tafel plots. (c) Electron transfer number and H_2O_2 yield for triNC, N-G and Pt/C, as calculated from RRDE. (d) The comparison of ORR performance and N contents of triNCs prepared at different carbonization temperatures. (e) Methanol tolerance performance and (f) long term durability of triNC and Pt/C.

The ORR activities of triNC (containing C-N2 sites), N-G (with C-N sites), and commercial Pt/C are evaluated using rotating-disk electrode (RDE) test using a three electrode system. All potentials are measured with respect to the reference hydrogen electrode (RHE). The ORR activities can be directly evaluated using CV curves (Figure S12). Compared with N-G (peak position: 0.762 V), triNC reveals better ORR performance with much more positive peak of oxygen reduction (0.853 V). This is even better than that of the performance with Pt/C (0.847 V). It clearly indicates that the triazine ring structure with unique C-N2 site possesses outstanding ORR activity. In fact it even outperforms the activity due to pyri-N groups and Pt/C.

The ORR activity is further evaluated using linear sweep voltammetry (LSV) at 1600 rpm (Figure 4a). Onset potential (0.98 V) and half-wave potential ($E_{1/2}$, 0.89 V) of triNC are significantly superior to those for N-G (0.88 V and 0.82 V) and Pt/C (0.95 V and 0.85 V). These results demonstrate the higher ORR activity of the C-N2 containing triNC when compared to other samples. This is in agreement with DFT based predictions made earlier in this work.

Furthermore, triNC reveals the lowest slope of Tafel plot (~113.3 mV dec^{-1}), indicating the lowest kinetic resistance to ORR (Figure 4b). Rotating ring disk electrode (RRDE) test is conducted to investigate the ORR mechanism. As shown in Figure S13, the disk current follows the trends consistent with the LSV curves. The electron transfer number and H_2O_2 yield calculated from the ring and disk current density are shown in Figure 4c. All three samples follow the $4e^-$ pathway during ORR; the H_2O_2 yields are less than 5%. The triNC exhibits the lowest peroxide yields of ~2.5%, suggesting the highest energy efficacy among all samples studied.

The influence of carbonization temperature during synthesis is also considered. It is clearly seen that the ORR performance improves with the increase in carbonization temperature. triNC1100 exhibits the best ORR performance. While heteroatom doping is evidently helpful, beyond a critical concentration, the conductivity of carbon matrix gets affected, which in turn is expected to lower ORR activity. [58-59] On the other hand, low N-doping leads to lack of sufficient number of active sites. It is necessary to find an appropriate balance between high conductivity and high content of activity sites via optimizing the content of N doping. Usually the N content decreases with increase of carbonization temperature which has great influences on the performance of final products. According to our experimental results, ORR performance of triNCs improves with the increasing of annealing temperature and reaches the top at 1100 °C. TriNC1100 with total N content of ~2.5 at% performs the best (Figure 4d, Figure S14-S15). This performance of triNC is evidently superior to those of most typical noble metal free ORR electrocatalysts reported in recent five years (Table S2).[4, 15, 17-21, 23-29, 60-67]

The methanol tolerance performance and durability of triNC are evaluated by chronoamperometry (*i-t* measurement, Figure 4e-f). During methanol tolerance test, methanol is added into the cell at 300 s and a sudden decrease of ORR current occurs. The current recovers slowly and remains at ~94.0% of original current. Tis is better than Pt/C (remaining 74.7% of original one). Also, triNC exhibits good long-term stability, and shows only 14.0 % activity loss after running for 8 h. In fact Pt/C shows a larger activity loss of ~19.1% under the identical condition.

DFT calculations are performed to yield mechanistic insights into the observed ORR activity on triNC and pyri-N doped carbon. The reaction pathway toward ORR on the surface of pyri-N and triNC is shown in Figure 5a-b (see details in SI). The Gibbs free energy for each primitive reaction occurring during ORR is calculated (Figure 5c-d). It is clearly seen that the rate determining step of ORR is the first reaction ($* + \mathrm{O_2} + \mathrm{H_2O} + e^- = *\mathrm{OOH} + \mathrm{OH}^-$ formation of *OOH). This is in fact related to the dissociation of O_2 on the surface and elsewhere also reported to the rate-limiting step of ORR.[47]

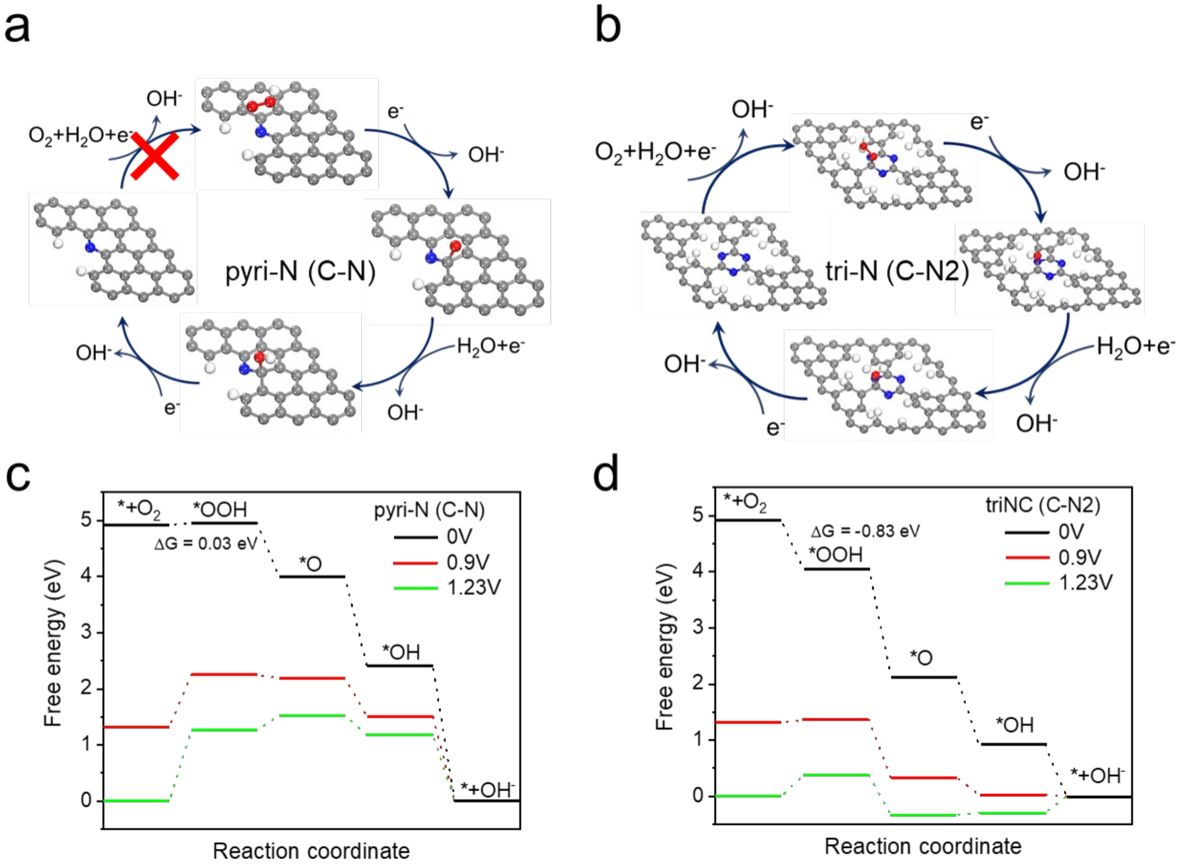

Figure 5. ORR mechanism. Schematic pathway of ORR on (a) pyri-N (C-N site) doped carbon and (b) triNC (C-N2 site). Grey, blue, red and white spheres represent C, N, O and H atoms, respectively. Free-energy paths of intermediates in ORR on (c) pyri-N doped carbon and (d) triazine ring doped carbon at different potential (0 V, 0.9 V and 1.23 V).

On pyri-N doped carbon (C-N), the intermediate OOH cannot be adsorbed onto the surface (C-OOH bond length: 3.34 Å), since such a step is endothermic (ΔG_{*OOH} = 0.03 eV, Figure S16b). On the other hand, on triNC (C-N2), the rather high oxygen binding energy accelerates the dissociation of oxygen. This in turn renders the formation of OOH intermediate on C-N2 spontaneous (ΔG_{*OOH} = -0.83 eV, C-OOH bond length: 1.53 Å, Figure S16a). Shorter C-OOH bond length and endothermic reaction path as well as better adsorption geometry indicating better ORR performance (Figure S17). When the applied potential is considered, it is clearly revealed that C-N2 goes through a much smoother reaction pathway at 0.9 V and equilibrium potential than C-N does. Therefore, it is reasonable that C-N2 in triNC contributes to superior ORR activity (when compared to C-N sites in N-G).

Finally, a Zn-air battery (ZAB) is assembled to evaluate the practical use of triNC. The mixture of triNC and NiFe layered double hydroxides (NiFe LDH, see detail in the supporting information) is sprayed onto carbon paper to serve as the cathode in a ZAB (Figure S17a). The ZAB provides an open circuit voltage of ~1.37 V. The charge and discharge polarization curve and corresponding power density are shown in Figure 6a and Figure S17b; triNC provides a power density of 74.4 mW cm^{-2}, which is larger than that of Pt/C (66.9 mW cm^{-2}). Also, the specific capacity of the ZAB is evaluated at a discharge density of 10 mA cm^{-2} (Figure 6b). The triNC based system exhibits a high specific capacitance (778.1 mAh g^{-1}), which is ~94.9% of theoretical capacitance (820 mAh g^{-1}, Figure 6b) and is higher than that of Pt/C-based ZAB (767.7 mAh g^{-1}). The energy density of triNC-based ZAB reaches 853.6 Wh Kg^{-1} (Figure S17c), and it outperforms Pt/C-based ZAB (819.1 Wh Kg^{-1}). The stability of triNC working in a rechargeable ZAB is evaluated by charge/discharge cycles (Figure 6c-d). The discharge platform of triNC overlaps that of Pt/C (~1.1 V) in first 20 h. However triNC exhibits better durability than commercial Pt/C does. After running for 80 h (160 cycles), triNC does not show any evidence of polarization. These results indicate the high potential for triNC to be served as the cathode material of metal-air battery.

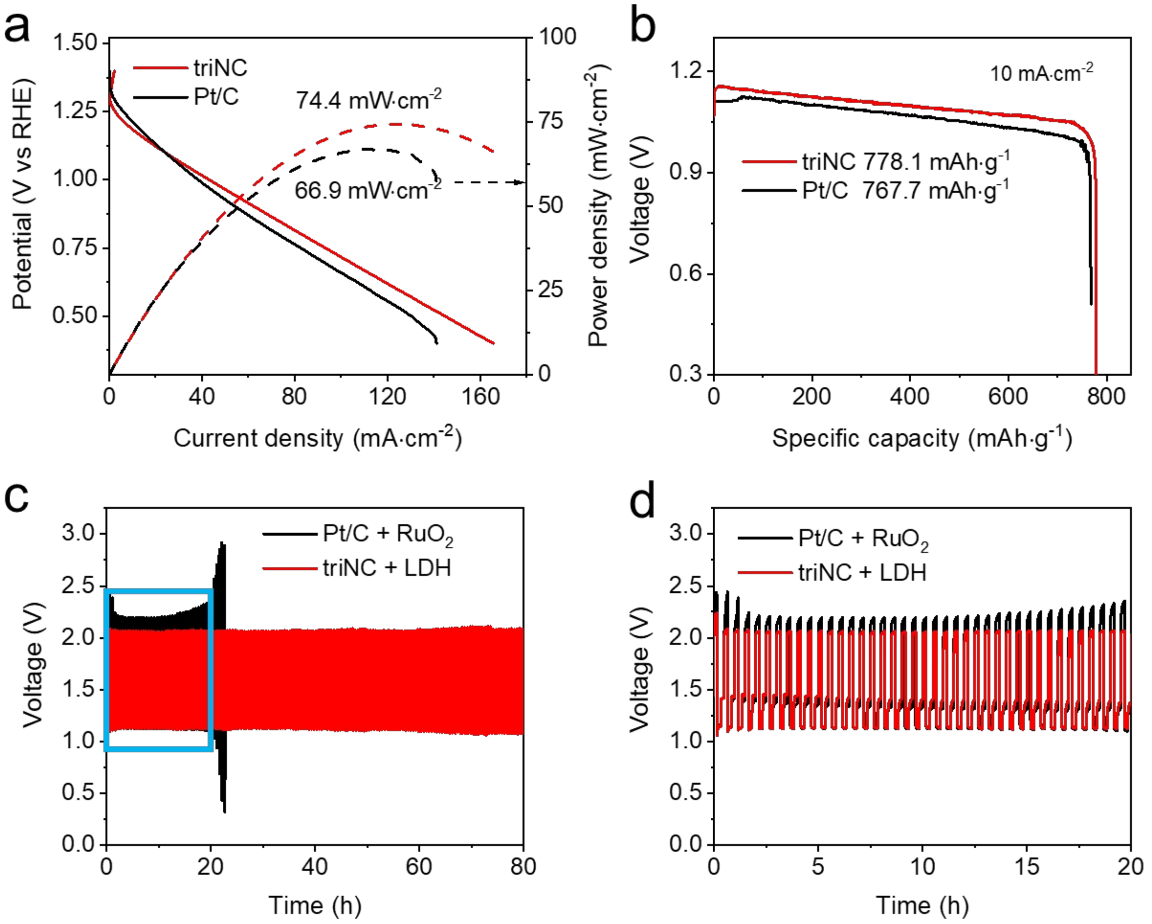

Figure 6. Zn-air battery (ZAB) measurements. (a) Discharge polarization curve and corresponding power density, and (b) Galvanostatic discharge voltage–capacity curves for primary ZAB using triNC or Pt/C. (c) Charge-discharge circling performance for rechargeable ZAB built using triNC + NiFe LDH and Pt/C + RuO_2. (d) The enlarged part in blue square box of panel (c).

3. Conclusion

In summary, we demonstrate a good N-doping strategy and an atomic-scale design approach to enhance the electrocatalytic ORR activity of carbon materials. The successful synthesis of triazine-ring-doped carbon (triNC) in which one carbon site is flanked by two N atoms (C-N2 site) is realized. This is done by carbonizing a covalent triazine framework at high temperatures. Both density functional theory calculations and electrochemical experiments confirm the fact that the C-N2 sites provide a means to achieve higher ORR activity in alkaline medium, when compared to the conventional C-N sites (pyridinic-N group) based materials and Pt/C. Noble metal-free Zn-air battery is assembled using a mixture of triNC and NiFe LDH that serves as the air cathode. The battery with this cathode provides higher power and energy density, and offers better stability than Pt/C+RuO_2. Hence the results prove the potential of triNC for practical applications. This strategy of designing triazine ring-doped carbons as active ORR electrocatalysts will open up fresh avenues for realizing other site-specific doped electrocatalysts relevant for energy conversion and storage.

Corresponding Author

*Ruguang Ma: maruguang@mail.sic.ac.cn

*Jiacheng Wang: jiacheng.wang@mail.sic.ac.cn

Author Contributions

The manuscript was written through contributions of all authors. All authors have given approval to the final version of the manuscript.

Supporting Information

The Supporting Information is available free of charge at https://pubs.acs.org/doi/

Details of experiment and DFT calculation, additional DOS of C-N and C-N2 with and without O adsorption, ^{13}C NMR of CTF, pore size distribution of triNCs, characterization of N-G (SEM, Raman spectrum, N_2 isothermal ad/desorption), additional XPS spectrum of triNCs and N-G, additional CV, LSV and RRDE curves of triNCs, N-G and Pt/C, additional Zn-air performances (charge and discharge curves and energy density).

ACKNOWLEDGMENT

The authors are grateful to the financial support from NSFC (51602332), and Technology Commission of Shanghai Municipality (16DZ2260603, 19ZR1465100, 19ZR1479500), and Equipment Research Program (6140721050215). M. Yang would like to thank the National 1000 Youth Talents program of China and financial support from Ningbo 3315 program. Tiju Thomas expresses thanks for support from DST Solar Energy Harnessing Centre, Ministry of Electronics and Information Technology, India (Project ID: ELE1819353MEITNAK), and DST (Project ID: MET1617146DSTXTIJU, Materials for Energy Storage, and DST/TMD/SERI/HUB/1(C)) for supporting this research work. WC acknowledges the support from U.S. National Science Foundation (NSF) under the CAREER award DMR-1945380.

REFERENCES

1. Yu, P.; Wang, L.; Sun, F.; Xie, Y.; Liu, X.; Ma, J.; Wang, X.; Tian, C.; Li, J.; Fu, H., Co Nanoislands Rooted on Co–N–C Nanosheets as Efficient Oxygen Electrocatalyst for Zn–Air Batteries. *Adv. Mater.* **2019,** *31*, 1901666.
2. Nagaiah, T. C.; Kundu, S.; Bron, M.; Muhler, M.; Schuhmann, W., Nitrogen-doped carbon nanotubes as a cathode catalyst for the oxygen reduction reaction in alkaline medium. *Electrochem. Commun.* **2010,** *12*, 338-341.
3. Guo, B.; Ma, R.; Li, Z.; Guo, S.; Luo, J.; Yang, M.; Liu, Q.; Thomas, T.; Wang, J., Hierarchical N-Doped Porous Carbons for Zn–Air Batteries and Supercapacitors. *Nano-Micro Lett.* **2020,** *12*, 20.
4. Lu, Q.; Yu, J.; Zou, X.; Liao, K.; Tan, P.; Zhou, W.; Ni, M.; Shao, Z., Self-Catalyzed Growth of Co, N-Codoped CNTs on Carbon-Encased CoSx Surface: A Noble-Metal-Free Bifunctional Oxygen Electrocatalyst for Flexible Solid Zn–Air Batteries. *Adv. Funct. Mater.* **2019,** *0*, 1904481.
5. Singh, S. K.; Takeyasu, K.; Nakamura, J., Active Sites and Mechanism of Oxygen Reduction Reaction Electrocatalysis on Nitrogen-Doped Carbon Materials. *Adv. Mater.* **2019,** *31*, 1804297.
6. Qiao, M.; Wang, Y.; Wang, Q.; Hu, G.; Mamat, X.; Zhang, S.; Wang, S., Hierarchically Ordered Porous Carbon with Atomically Dispersed FeN4 for Ultraefficient Oxygen Reduction Reaction in Proton-Exchange Membrane Fuel Cells. *Angew. Chem. Int. Ed.* **2020,** *59*, 2688-2694.
7. Liu, K.; Qiao, Z.; Hwang, S.; Liu, Z.; Zhang, H.; Su, D.; Xu, H.; Wu, G.; Wang, G., Mn- and N- doped carbon as promising catalysts for oxygen reduction reaction: Theoretical prediction and experimental validation. *Appl. Catal. B* **2019,** *243*, 195-203.
8. Yang, L.; Shui, J.; Du, L.; Shao, Y.; Liu, J.; Dai, L.; Hu, Z., Carbon-Based Metal-Free ORR Electrocatalysts for Fuel Cells: Past, Present, and Future. *Adv. Mater.* **2019,** *31*, 1804799.
9. Ma, R.; Lin, G.; Zhou, Y.; Liu, Q.; Zhang, T.; Shan, G.; Yang, M.; Wang, J., A review of oxygen reduction mechanisms for metal-free carbon-based electrocatalysts. *NPJ Comput. Mater.* **2019,** *5*, 78.
10. Hu, Y.; Ma, R.; Ju, Q.; Guo, B.; Yang, M.; Liu, Q.; Wang, J., S, N dual-doped porous carbon materials derived from biomass for Na ion storage and O2 electroreduction. *Microporous Mesoporous Mater.* **2020,** *294*, 109930.

11. Xing, R.; Zhou, T.; Zhou, Y.; Ma, R.; Liu, Q.; Luo, J.; Wang, J., Creation of Triple Hierarchical Micro-Meso-Macroporous N-doped Carbon Shells with Hollow Cores Toward the Electrocatalytic Oxygen Reduction Reaction. *Nano-Micro Lett.* **2017,** *10*, 3.
12. Gong, K.; Du, F.; Xia, Z.; Durstock, M.; Dai, L., Nitrogen-Doped Carbon Nanotube Arrays with High Electrocatalytic Activity for Oxygen Reduction. *Science* **2009,** *323*, 760.
13. Luo, Z.; Lim, S.; Tian, Z.; Shang, J.; Lai, L.; MacDonald, B.; Fu, C.; Shen, Z.; Yu, T.; Lin, J., Pyridinic N doped graphene: synthesis, electronic structure, and electrocatalytic property. *J. Mater. Chem.* **2011,** *21*, 8038-8044.
14. Yan, X.; Jia, Y.; Odedairo, T.; Zhao, X.; Jin, Z.; Zhu, Z.; Yao, X., Activated carbon becomes active for oxygen reduction and hydrogen evolution reactions. *Chem. Commun.* **2016,** *52*, 8156-8159.
15. Zhao, Y.; Wan, J.; Yao, H.; Zhang, L.; Lin, K.; Wang, L.; Yang, N.; Liu, D.; Song, L.; Zhu, J.; Gu, L.; Liu, L.; Zhao, H.; Li, Y.; Wang, D., Few-layer graphdiyne doped with sp-hybridized nitrogen atoms at acetylenic sites for oxygen reduction electrocatalysis. *Nat. Chem.* **2018,** *10*, 924-931.
16. Zhu, J.; Xiao, M.; Song, P.; Fu, J.; Jin, Z.; Ma, L.; Ge, J.; Liu, C.; Chen, Z.; Xing, W., Highly polarized carbon nano-architecture as robust metal-free catalyst for oxygen reduction in polymer electrolyte membrane fuel cells. *Nano Energy* **2018,** *49*, 23-30.
17. Peng, X.; Zhang, L.; Chen, Z.; Zhong, L.; Zhao, D.; Chi, X.; Zhao, X.; Li, L.; Lu, X.; Leng, K.; Liu, C.; Liu, W.; Tang, W.; Loh, K. P., Hierarchically Porous Carbon Plates Derived from Wood as Bifunctional ORR/OER Electrodes. *Adv. Mater.* **2019,** *31*, 1900341.
18. Wu, H.; Geng, J.; Ge, H.; Guo, Z.; Wang, Y.; Zheng, G., Egg-Derived Mesoporous Carbon Microspheres as Bifunctional Oxygen Evolution and Oxygen Reduction Electrocatalysts. *Adv. Energy Mater.* **2016,** *6*, 1600794.
19. Shinde, S. S.; Lee, C.-H.; Sami, A.; Kim, D.-H.; Lee, S.-U.; Lee, J.-H., Scalable 3-D Carbon Nitride Sponge as an Efficient Metal-Free Bifunctional Oxygen Electrocatalyst for Rechargeable Zn–Air Batteries. *ACS Nano* **2017,** *11*, 347-357.
20. Wu, M.; Wang, Y.; Wei, Z.; Wang, L.; Zhuo, M.; Zhang, J.; Han, X.; Ma, J., Ternary doped porous carbon nanofibers with excellent ORR and OER performance for zinc–air batteries. *J. Mater. Chem. A* **2018,** *6*, 10918-10925.
21. Ye, L.; Chai, G.; Wen, Z., Zn-MOF-74 Derived N-Doped Mesoporous Carbon as pH-Universal Electrocatalyst for Oxygen Reduction Reaction. *Adv. Funct. Mater.* **2017,** *27*, 1606190.
22. Zhang, L.; Xia, Z., Mechanisms of Oxygen Reduction Reaction on Nitrogen-Doped Graphene for Fuel Cells. *J. Phys. Chem. C* **2011,** *115*, 11170-11176.
23. Meng, Z.; Cai, S.; Wang, R.; Tang, H.; Song, S.; Tsiakaras, P., Bimetallic−organic framework-derived hierarchically porous Co-Zn-N-C as efficient catalyst for acidic oxygen reduction reaction. *Appl. Catal. B* **2019,** *244*, 120-127.
24. Wan, K.; Tan, A.-d.; Yu, Z.-p.; Liang, Z.-x.; Piao, J.-h.; Tsiakaras, P., 2D nitrogen-doped hierarchically porous carbon: Key role of low dimensional structure in favoring electrocatalysis and mass transfer for oxygen reduction reaction. *Appl. Catal. B* **2017,** *209*, 447-454.
25. Wang, K.; Chen, H.; Zhang, X.; Tong, Y.; Song, S.; Tsiakaras, P.; Wang, Y., Iron oxide@graphitic carbon core-shell nanoparticles embedded in ordered mesoporous N-doped carbon matrix as an efficient cathode catalyst for PEMFC. *Appl. Catal. B* **2020,** *264*, 118468.
26. Wang, Y.; Liu, H.; Wang, K.; Song, S.; Tsiakaras, P., 3D interconnected hierarchically porous N-doped carbon with NH3 activation for efficient oxygen reduction reaction. *Appl. Catal. B* **2017,** *210*, 57-66.
27. Tan, A.-D.; Wan, K.; Wang, Y.-F.; Fu, Z.-Y.; Liang, Z.-X., N, S-containing MOF-derived dual-doped mesoporous carbon as a highly effective oxygen reduction reaction electrocatalyst. *Catal. Sci. Technol.* **2018,** *8*, 335-343.
28. Lyu, D.; Mollamahale, Y. B.; Huang, S.; Zhu, P.; Zhang, X.; Du, Y.; Wang, S.; Qing, M.; Tian, Z. Q.; Shen, P. K., Ultra-high surface area graphitic Fe-N-C nanospheres with single-atom iron sites as highly efficient non-precious metal bifunctional catalysts towards oxygen redox reactions. *J. Catal.* **2018,** *368*, 279-290.

29. Zhang, X.; Mollamahale, Y. B.; Lyu, D.; Liang, L.; Yu, F.; Qing, M.; Du, Y.; Zhang, X.; Tian, Z. Q.; Shen, P. K., Molecular-level design of Fe-N-C catalysts derived from Fe-dual pyridine coordination complexes for highly efficient oxygen reduction. *J. Catal.* **2019,** *372*, 245-257.
30. Jia, Y.; Zhang, L.; Du, A.; Gao, G.; Chen, J.; Yan, X.; Brown, C. L.; Yao, X., Defect Graphene as a Trifunctional Catalyst for Electrochemical Reactions. *Adv. Mater.* **2016,** *28*, 9532-9538.
31. Tao, L.; Qiao, M.; Jin, R.; Li, Y.; Xiao, Z.; Wang, Y.; Zhang, N.; Xie, C.; He, Q.; Jiang, D.; Yu, G.; Li, Y.; Wang, S., Bridging the Surface Charge and Catalytic Activity of a Defective Carbon Electrocatalyst. *Angew. Chem. Int. Ed.* **2019,** *58*, 1019-1024.
32. Zhu, J.; Huang, Y.; Mei, W.; Zhao, C.; Zhang, C.; Zhang, J.; Amiinu, I. S.; Mu, S., Effects of Intrinsic Pentagon Defects on Electrochemical Reactivity of Carbon Nanomaterials. *Angew. Chem. Int. Ed.* **2019,** *58*, 3859-3864.
33. Jia, Y.; Zhang, L.; Zhuang, L.; Liu, H.; Yan, X.; Wang, X.; Liu, J.; Wang, J.; Zheng, Y.; Xiao, Z.; Taran, E.; Chen, J.; Yang, D.; Zhu, Z.; Wang, S.; Dai, L.; Yao, X., Identification of active sites for acidic oxygen reduction on carbon catalysts with and without nitrogen doping. *Nature Catal.* **2019,** *2*, 688-695.
34. Dai, L.; Xue, Y.; Qu, L.; Choi, H.-J.; Baek, J.-B., Metal-Free Catalysts for Oxygen Reduction Reaction. *Chem. Rev.* **2015,** *115*, 4823-4892.
35. Li, D.; Jia, Y.; Chang, G.; Chen, J.; Liu, H.; Wang, J.; Hu, Y.; Xia, Y.; Yang, D.; Yao, X., A Defect-Driven Metal-free Electrocatalyst for Oxygen Reduction in Acidic Electrolyte. *Chem* **2018,** *4*, 2345-2356.
36. Zhao, H.; Sun, C.; Jin, Z.; Wang, D.-W.; Yan, X.; Chen, Z.; Zhu, G.; Yao, X., Carbon for the oxygen reduction reaction: a defect mechanism. *J. Mater. Chem. A* **2015,** *3*, 11736-11739.
37. Guo, D.; Shibuya, R.; Akiba, C.; Saji, S.; Kondo, T.; Nakamura, J., Active sites of nitrogen-doped carbon materials for oxygen reduction reaction clarified using model catalysts. *Science* **2016,** *351*, 361.
38. Li, Y.; Zheng, S.; Liu, X.; Li, P.; Sun, L.; Yang, R.; Wang, S.; Wu, Z.-S.; Bao, X.; Deng, W.-Q., Conductive Microporous Covalent Triazine-Based Framework for High-Performance Electrochemical Capacitive Energy Storage. *Angew. Chem. Int. Ed.* **2018,** *57*, 7992-7996.
39. Kuhn, P.; Antonietti, M.; Thomas, A., Porous, Covalent Triazine-Based Frameworks Prepared by Ionothermal Synthesis. *Angew. Chem. Int. Ed.* **2008,** *47*, 3450-3453.
40. Sidik, R. A.; Anderson, A. B.; Subramanian, N. P.; Kumaraguru, S. P.; Popov, B. N., O2 Reduction on Graphite and Nitrogen-Doped Graphite: Experiment and Theory. *J. Phys. Chem. B* **2006,** *110*, 1787-1793.
41. Zhang, L.; Niu, J.; Dai, L.; Xia, Z., Effect of Microstructure of Nitrogen-Doped Graphene on Oxygen Reduction Activity in Fuel Cells. *Langmuir* **2012,** *28*, 7542-7550.
42. Jeon, I.-Y.; Zhang, S.; Zhang, L.; Choi, H.-J.; Seo, J.-M.; Xia, Z.; Dai, L.; Baek, J.-B., Edge-Selectively Sulfurized Graphene Nanoplatelets as Efficient Metal-Free Electrocatalysts for Oxygen Reduction Reaction: The Electron Spin Effect. *Adv. Mater.* **2013,** *25*, 6138-6145.
43. Yang, L.; Cheng, D.; Xu, H.; Zeng, X.; Wan, X.; Shui, J.; Xiang, Z.; Cao, D., Unveiling the high-activity origin of single-atom iron catalysts for oxygen reduction reaction. *Proc. Natl. Acad. Sci. U.S.A.* **2018,** *115*, 6626.
44. Zhang, G.; Duan, W.; Gu, B., Effect of substitutional atoms in the tip on field-emission properties of capped carbon nanotubes. *Appl. Phys. Lett.* **2002,** *80*, 2589-2591.
45. Maldonado, S.; Stevenson, K. J., Influence of Nitrogen Doping on Oxygen Reduction Electrocatalysis at Carbon Nanofiber Electrodes. *J. Phys. Chem. B* **2005,** *109*, 4707-4716.
46. Sun, Y. Y.; Kim, Y.-H.; Zhang, S. B., Effect of Spin State on the Dihydrogen Binding Strength to Transition Metal Centers in Metal-Organic Frameworks. *J. Am. Chem. Soc.* **2007,** *129*, 12606-12607.
47. Nørskov, J. K.; Rossmeisl, J.; Logadottir, A.; Lindqvist, L.; Kitchin, J. R.; Bligaard, T.; Jónsson, H., Origin of the Overpotential for Oxygen Reduction at a Fuel-Cell Cathode. *J. Phys. Chem. B* **2004,** *108*, 17886-17892.

48. Zhou, S.; Liu, N.; Wang, Z.; Zhao, J., Nitrogen-Doped Graphene on Transition Metal Substrates as Efficient Bifunctional Catalysts for Oxygen Reduction and Oxygen Evolution Reactions. *ACS Appl. Mater. Interfaces* **2017,** *9*, 22578-22587.
49. Huang, W.; He, Q.; Hu, Y.; Li, Y., Molecular Heterostructures of Covalent Triazine Frameworks for Enhanced Photocatalytic Hydrogen Production. *Angew. Chem. Int. Ed.* **2019,** *58*, 8676-8680.
50. Yu, S.-Y.; Mahmood, J.; Noh, H.-J.; Seo, J.-M.; Jung, S.-M.; Shin, S.-H.; Im, Y.-K.; Jeon, I.-Y.; Baek, J.-B., Direct Synthesis of a Covalent Triazine-Based Framework from Aromatic Amides. *Angew. Chem. Int. Ed.* **2018,** *57*, 8438-8442.
51. Osada, Y.; Yu, Q. S.; Yasunaga, H.; Wang, F. S.; Chen, J., Preparation and electrical properties of polymeric TCNQ and TCNE films by plasma polymerization. *J. Appl. Phys.* **1988,** *64*, 1476-1483.
52. Hao, L.; Ning, J.; Luo, B.; Wang, B.; Zhang, Y.; Tang, Z.; Yang, J.; Thomas, A.; Zhi, L., Structural Evolution of 2D Microporous Covalent Triazine-Based Framework toward the Study of High-Performance Supercapacitors. *J. Am. Chem. Soc.* **2015,** *137*, 219-225.
53. Ferrari, A. C.; Robertson, J., Interpretation of Raman spectra of disordered and amorphous carbon. *Phys. Rev. B* **2000,** *61*, 14095-14107.
54. Schwan, J.; Ulrich, S.; Batori, V.; Ehrhardt, H.; Silva, S. R. P., Raman spectroscopy on amorphous carbon films. *J. Appl. Phys.* **1996,** *80*, 440-447.
55. Wang, Q.; Li, H.; Chen, L.; Huang, X., Monodispersed hard carbon spherules with uniform nanopores. *Carbon* **2001,** *39*, 2211-2214.
56. Jagiello, J.; Kenvin, J.; Olivier, J. P.; Lupini, A. R.; Contescu, C. I., Using a New Finite Slit Pore Model for NLDFT Analysis of Carbon Pore Structure. *Adsorp. Sci. Technol.* **2011,** *29*, 769-780.
57. Lin, Z.; Yang, Y.; Li, M.; Huang, H.; Hu, W.; Cheng, L.; Yan, W.; Yu, Z.; Mao, K.; Xia, G.; Lu, J.; Jiang, P.; Yang, K.; Zhang, R.; Xu, P.; Wang, C.; Hu, L.; Chen, Q., Dual Graphitic-N Doping in a Six-Membered C-Ring of Graphene-Analogous Particles Enables an Efficient Electrocatalyst for the Hydrogen Evolution Reaction. *Angew. Chem. Int. Ed.* **2019,** *58*, 16973-16980.
58. Fujisawa, K.; Tojo, T.; Muramatsu, H.; Elías, A. L.; Vega-Díaz, S. M.; Tristán-López, F.; Kim, J. H.; Hayashi, T.; Kim, Y. A.; Endo, M.; Terrones, M., Enhanced electrical conductivities of N-doped carbon nanotubes by controlled heat treatment. *Nanoscale* **2011,** *3*, 4359-4364.
59. Ismagilov, Z. R.; Shalagina, A. E.; Podyacheva, O. Y.; Ischenko, A. V.; Kibis, L. S.; Boronin, A. I.; Chesalov, Y. A.; Kochubey, D. I.; Romanenko, A. I.; Anikeeva, O. B.; Buryakov, T. I.; Tkachev, E. N., Structure and electrical conductivity of nitrogen-doped carbon nanofibers. *Carbon* **2009,** *47*, 1922-1929.
60. Thomas, M.; Illathvalappil, R.; Kurungot, S.; Nair, B. N.; Mohamed, A. A. P.; Anilkumar, G. M.; Yamaguchi, T.; Hareesh, U. S., Graphene Oxide Sheathed ZIF-8 Microcrystals: Engineered Precursors of Nitrogen-Doped Porous Carbon for Efficient Oxygen Reduction Reaction (ORR) Electrocatalysis. *ACS Appl. Mater. Interfaces* **2016,** *8*, 29373-29382.
61. Hou, C.-C.; Zou, L.; Xu, Q., A Hydrangea-Like Superstructure of Open Carbon Cages with Hierarchical Porosity and Highly Active Metal Sites. *Adv. Mater.* **2019,** *31*, 1904689.
62. Zhang, X.; Liu, R.; Zang, Y.; Liu, G.; Wang, G.; Zhang, Y.; Zhang, H.; Zhao, H., Co/CoO nanoparticles immobilized on Co–N-doped carbon as trifunctional electrocatalysts for oxygen reduction, oxygen evolution and hydrogen evolution reactions. *Chem. Commun.* **2016,** *52*, 5946-5949.
63. Jiang, H.; Gu, J.; Zheng, X.; Liu, M.; Qiu, X.; Wang, L.; Li, W.; Chen, Z.; Ji, X.; Li, J., Defect-rich and ultrathin N doped carbon nanosheets as advanced trifunctional metal-free electrocatalysts for the ORR, OER and HER. *Energy Environ. Sci.* **2019,** *12*, 322-333.
64. Pei, Z.; Li, H.; Huang, Y.; Xue, Q.; Huang, Y.; Zhu, M.; Wang, Z.; Zhi, C., Texturing in situ: N,S-enriched hierarchically porous carbon as a highly active reversible oxygen electrocatalyst. *Energy Environ. Sci.* **2017,** *10*, 742-749.

65. Liu, L.; Zeng, G.; Chen, J.; Bi, L.; Dai, L.; Wen, Z., N-doped porous carbon nanosheets as pH-universal ORR electrocatalyst in various fuel cell devices. *Nano Energy* **2018,** *49*, 393-402.
66. Zhang, J.; Zhao, Z.; Xia, Z.; Dai, L., A metal-free bifunctional electrocatalyst for oxygen reduction and oxygen evolution reactions. *Nat. Nanotechnol.* **2015,** *10*, 444.
67. Lyu, D.; Du, Y.; Huang, S.; Mollamahale, B. Y.; Zhang, X.; Hasan, S. W.; Yu, F.; Wang, S.; Tian, Z. Q.; Shen, P. K., Highly Efficient Multifunctional Co–N–C Electrocatalysts with Synergistic Effects of Co–N Moieties and Co Metallic Nanoparticles Encapsulated in a N-Doped Carbon Matrix for Water-Splitting and Oxygen Redox Reactions. *ACS Appl. Mater. Interfaces* **2019,** *11*, 39809-39819.

For Table of Content only